IEEE Access
Multidisciplinary | Rapid Review | Open Access Journal

Received April 14, 2021, accepted May 1, 2021, date of publication May 4, 2021, date of current version May 25, 2021.

Digital Object Identifier 10.1109/ACCESS.2021.3077561

Fractional-Order Inductor: Design, Simulation, and Implementation

LI ZHANG[1], (Student Member, IEEE), ASLIHAN KARTCI[1], (Member, IEEE), AHMED ELWAKIL[2], (Senior Member, IEEE), HAKAN BAGCI[3], (Senior Member, IEEE), AND KHALED N. SALAMA[1], (Senior Member, IEEE)

[1]Sensors Laboratory, Computer, Electrical, and Mathematical Science and Engineering (CEMSE) Division, Advanced Membranes and Porous Materials Center (AMPMC), King Abdullah University of Science and Technology (KAUST), Thuwal 23955-6900, Saudi Arabia
[2]Department of Electrical and Computer Engineering, University of Sharjah, Sharjah, United Arab Emirates
[3]Computational Electromagnetics Group, Computer, Electrical, and Mathematical Science and Engineering (CEMSE) Division, King Abdullah University of Science and Technology (KAUST), Thuwal 23955-6900, Saudi Arabia

Corresponding author: Khaled N. Salama (khaled.salama@kaust.edu.sa)

This work was supported by the King Abdullah University of Science and Technology (KAUST), Thuwal, Saudi Arabia.

ABSTRACT Fractional calculus has tremendous potential in modeling the evolution of complex systems including those with memory. Indeed, fractional-order models are more accurate in approximating non-locally distributed dynamics with short- or long-term memory effects. However, the realization of fractional systems is often hindered by the lack of robust fractional-order energy storage devices, particularly fractional-order inductors (FOIs). Inherent eddy currents, hysteresis losses, the lack of suitable materials, and a systematic design procedure are among the challenges of FOI synthesis. In this work, a straightforward and robust approach realizing FOIs with a coaxial structure is proposed. This approach relies on the fact that the wave impedance of the transverse electromagnetic (TEM) mode on the coaxial structure scales with $(j\omega)^{0.5}$, where $j = \sqrt{(-1)}$ and ω is the angular frequency when the filling material is highly conductive. Indeed, experimental characterization of the realized device shows that it has a half-order inductive response (corresponding to 45° phase angle) that is stable in the frequency range 18 MHz – 1 GHz with a phase angle deviation not exceeding 5°. Furthermore, the effects of the device geometry and the permeability, the permittivity, the conductivity of the filling material on device response are investigated.

INDEX TERMS Coaxial cable, coil, electromagnetic fields, fractional-order circuits, fractional-order inductor, fractional-order resonator.

I. INTRODUCTION

Various electro- and bio-chemical systems, such as electrode-electrolyte polarization [1], [2], dielectric polarization [3], and electromagnetic waves [4] on certain geometries, exhibit a wide range of fractional-order behaviors. Modeling these systems with fractional calculus (FC) is not only more accurate, but is more adequate than integer-order models [5]–[7]. Indeed, fractional-order derivatives provide an excellent tool to describe memory and hereditary properties [8], [9]. Moreover, defining a system as fractional-order gives extra degrees of freedom in the form of arbitrary fractional-orders.

The associate editor coordinating the review of this manuscript and approving it for publication was Guido Lombardi.

Fractional-order derivative or integral operators can be realized physically using fractional-order capacitors and inductors. Figure 1 shows a comparison between ideal inductors/capacitors and fractional-order inductors (FOIs)/fractional-order capacitors (FOCs). Several fabrication techniques have been developed to design and realize single- and multi-component FOIs [10]–[13] and FOCs [14]–[24]. However, most of these techniques are focused on FOCs and none of them is industrialized yet. The studies in [25]–[29] show that FOCs and FOIs may have very practical uses in the industry, and therefore we believe that simple but rigorous methods are needed to fabricate them. An FOI using magnetorheological fluid as the core in a transformer-like device has been proposed [11], but this approach has a high fabrication complexity. A non-linear electrical inductor has

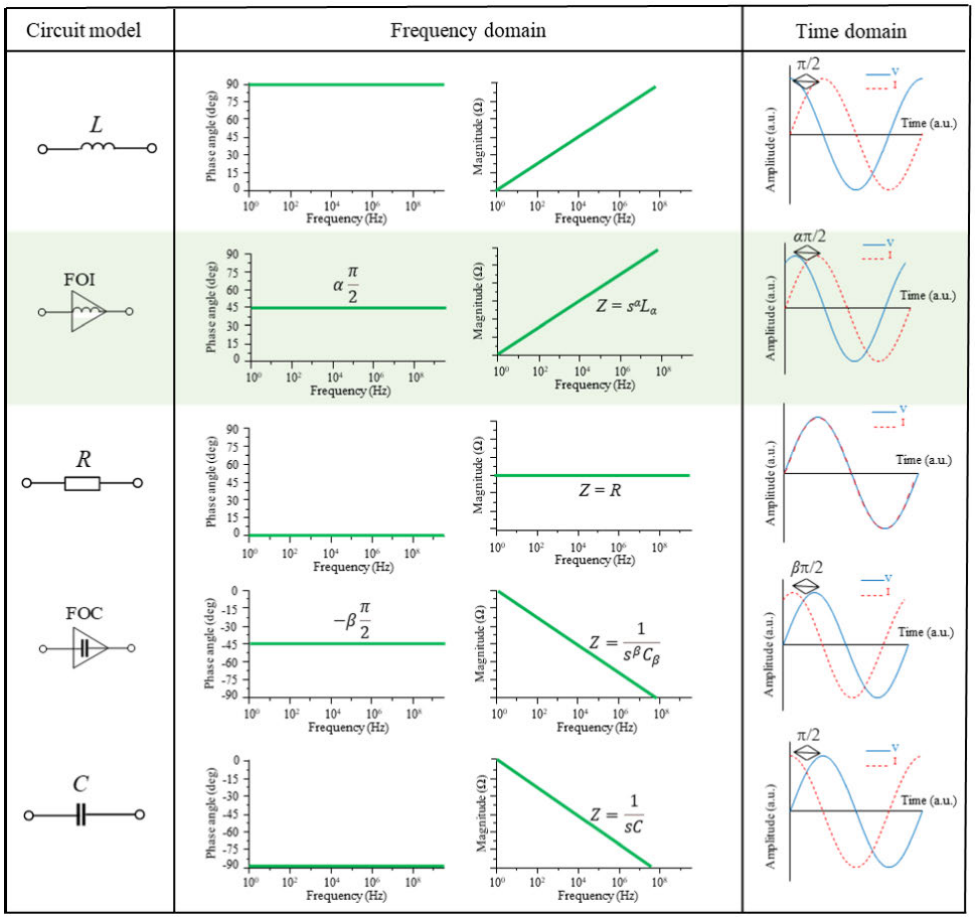

FIGURE 1. Comparison between conventional electrical elements and fractional-order ones. α and β are the order of the FOI and FOC, L is the inductance of the conventional inductor, L_{α} is the pseudo-inductance of the FOI, C is the capacitance of the conventional capacitor, C_{β} is the pseudo-capacitance of the FOC.

been experimentally characterized and FC has been used to model the dynamics of this device [30].

Westerlund *et al.* in 1994 has proposed a new model [31] that is based on the universal dielectric response. This model states that the current $i(t)$ through an inductor is given by:

$$v(t) = L_{\alpha}\frac{d^{\alpha}i(t)}{dt^{\alpha}}, \tag{1}$$

where $\frac{d^{\alpha}i(t)}{dt^{\alpha}}$ denotes the ''fractional-order time derivative'', $v(t)$ is the voltage on the inductor, α is the fractional-order ($0 < \alpha < 1$, $\alpha \in R$) that is related to ''proximity effect'' [32], and L_{α} is the fractional-order inductance with the unit of $H{\cdot}s^{\alpha-1}$. In the Laplace domain, the impedance of the inductor is given by $Z(s) = L_{\alpha}s^{\alpha}$, where $s = j\omega$, $j = \sqrt{(-1)}$, and ω is the angular frequency. Note that the phase angle of $Z(s)$ (in radians) is given by $\phi = \alpha\pi/2$. The slope of the logarithmic amplitude-frequency characteristic curve of the FOI is 20α dB/dec. In reality, ϕ depends on frequency, therefore to characterize the frequency dependence of an FOI, two quantities are defined: 1) constant phase zone (CPZ) as the frequency range where ϕ (or α) stays constant, 2) phase angle deviation (PAD): maximum deviation of ϕ (or α) from its constant value within the CPZ.

Several works on electromagnetic waves/fields with FOI characteristics have been presented in the literature. For example, the fractional wave equation (which shows the differences between fractal space-time geometry and classical models) in a conducting material has been described [33]. Similarly, fractional waves in dielectric media modeled using the Caputo fractional derivative have been discussed [34] and it has been shown that the amplitude of the electromagnetic field varies under different orders of the spatial and temporal fractional-order derivatives. A fractional-order wireless electric energy transmission system has been introduced recently [35]. By employing FOIs and FOCs to realize wireless power transmission, higher transmission efficiency and output power have been obtained. The fractional-order inductive phenomena based on the skin effect has been studied [36]. Transmission lines are modeled by fractional telegraph equations and the fractional-order partial differential equations are solved using the Laplace transform method [37]. Moreover, the ferromagnetic core coils can be modeled by fractional-order derivates independently than

the external wiring and frequency. A table of various coils and their fractional-orders α are described [38]. It is evident that off-the-self commercial coils show a response characteristic that differs from that of an integer-order inductance. However, the devices in [11], [30], [38] does not show the FOI characteristics by design and have no control on any parameters. Having said that, there exists a plethora of techniques developed to approximate/model FOI behavior using (i) passive elements (R-L trees) [12], [39], (ii) active elements [19], [40], [41], (iii) field programmable gate arrays (FPGA) [42], and (iv) field programmable analogue arrays (FPAA) [43], emulators and (v) generalized impedance converter (GIC) [44], [45]. Thus, to the best of the authors' knowledge, a systematic way of designing a passive single-component FOI has not been developed yet due to the challenges in modeling and fabrication.

In this work, we develop a straightforward and robust method to design a passive and single-component FOI for the first time in the literature. The method uses a coaxial structure filled with a highly conductive material. The high conductivity ensures that (a) transverse electromagnetic (TEM) mode of the coaxial structure under magneto-quasi-static (MQS) condition has a wave impedance that scales with $(j\omega)^{0.5}$ and (b) there are no reflections from the end of the structure. These two properties yield a lumped impedance with a fractional-order inductive response of $\phi = 45°$. This design method is verified via simulations using COMSOL Multiphysics® 5.5 program and via experimental characterization of the realized device. The effects of the device geometry and the permittivity ϵ, permeability μ, and conductivity σ of the filling material on the device response are discussed. Closed-form solutions of the characteristics are provided. The performance of the proposed FOI is verified through its application in the fractional-order parallel $RL_\alpha C$ resonance circuit.

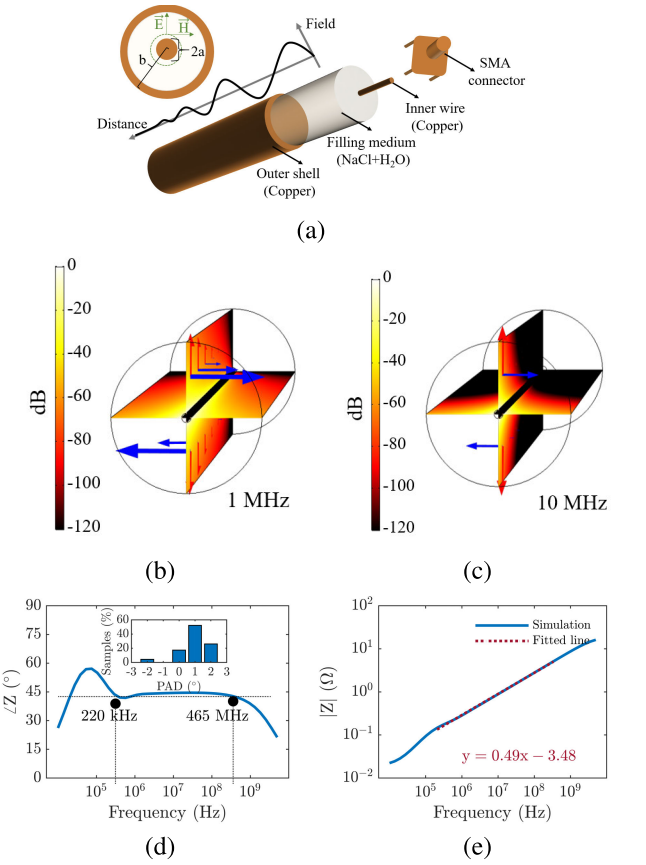

FIGURE 2. (a) Structure of the proposed design with a cross-section view and the profile of the strength of the fields. Simulated electric field norm of the proposed design with electric $\vec{E}$ field vectors (red arrow) and magnetic $\vec{H}$ field vectors (blue arrow) at working frequencies of (b) 1 MHz and (c) 10 MHz, (d) simulated phase angle response of the impedance for the proposed design with a histogram of the PAD shown in the inset, (e) simulated amplitude response of the impedance for the proposed design with a linear fit (red dash line) performed to the amplitude of the impedance.

II. DESIGN

The proposed design method generates the fractional inductance response via the TEM mode generated on a coaxial structure filled with a highly conductive material as shown in Fig. 2(a). Assuming the reflection from the end of the coaxial structure is small and ignoring the fringing effects, the magnetic and electric fields, $\vec{H}$ and $\vec{E}$, of the TEM mode are expressed as:

$$\vec{H} = \frac{A_0 e^{-\gamma z}}{\rho}\hat{\boldsymbol{\varphi}},$$
$$\vec{E} = \sqrt{\frac{j\omega\mu}{j\omega\epsilon+\sigma}}\frac{A_0 e^{-\gamma z}}{\rho}\hat{\boldsymbol{\rho}}. \quad (2)$$

In (2), A_0 is an arbitrary constant and $\hat{\boldsymbol{\rho}}$ and $\hat{\boldsymbol{\varphi}}$ are the unit vectors along the radial coordinate ($\boldsymbol{\rho}$) and the angular coordinate ($\boldsymbol{\varphi}$) on the cross-section (perpendicular to $\hat{z}$ direction). It is assumed that permittivity ϵ, permeability μ, and conductivity σ are constants. Also, $\gamma = \sqrt{j\omega\mu(j\omega\epsilon+\sigma)}$ is the propagation constant of the TEM mode. Integrating $\vec{H}$ along the $\hat{\boldsymbol{\varphi}}$ direction and integrating $\vec{E}$ along $\hat{\boldsymbol{\rho}}$ (both at $z = 0$) yield the current I and the voltage V at the feed of the coaxial structure as:

$$I = 2\pi A_0,$$
$$V = \sqrt{\frac{j\omega\mu}{j\omega\epsilon+\sigma}}A_0 ln(\frac{b}{a}). \quad (3)$$

Accordingly, the impedance at the feed can be obtained as:

$$Z = \frac{V}{I} = \frac{1}{2\pi}\sqrt{\frac{j\omega\mu}{j\omega\epsilon+\sigma}}ln(\frac{b}{a}). \quad (4)$$

Within the frequency of interest, $\sigma \gg \omega\epsilon$ (MQS approximation) and therefore the expression for impedance in (4) reduces to [46]:

$$Z = \frac{1}{2\pi}\sqrt{\frac{j\omega\mu}{\sigma}}ln(\frac{b}{a}) \propto (j\omega)^{0.5}. \quad (5)$$

Equation (5) shows that at low frequencies the impedance of the coaxial structure scales with $(j\omega)^{0.5}$ leading to a

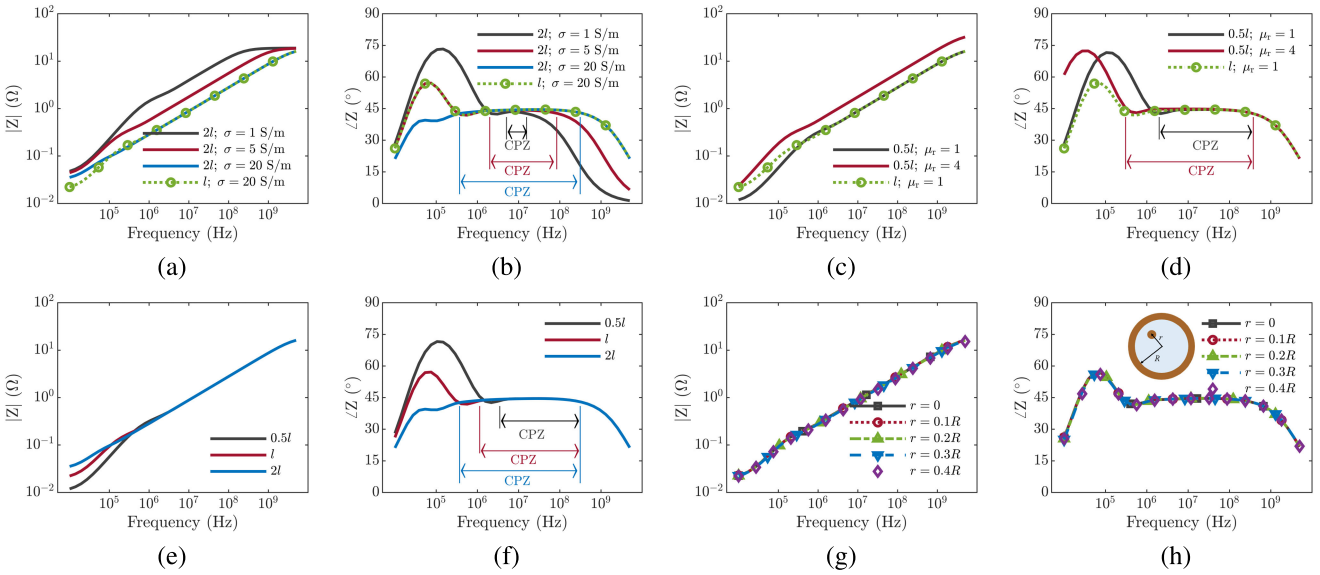

FIGURE 3. Simulated amplitude and phase angle of the impedance with: (a), (b) Two times of the device length and different conductivities of the filling medium, compared with the original case (green circle), (c), (d) half of the device length and different permeabilities of the filling medium, compared with the original case (green circle), (e), (f) different device lengths, (g), (h) different deviations of the core wire from the center of the coaxial structure. CPZs are highlighted.

half-order inductance behavior. It should also be noted here that under the MQS approximation, the expression for the propagation constant γ reduces to [46]:

$$\gamma = \frac{\sqrt{\omega\mu\sigma}}{2} + j\frac{\sqrt{\omega\mu\sigma}}{2}. \tag{6}$$

To verify the half-order fractional inductive response, the coaxial structure in Fig. 2(a) is simulated using COMSOL Multiphysics® 5.5. The inner radius, outer radius, and the length of the structure are set to $a = 0.275$ mm, $b = 4.47$ mm, and $l = 30$ cm, respectively. The filler material is NaCl water solution with relative permittivity $\epsilon_r = 78.4$, conductivity $\sigma = 20$ S/m, and relative permeability $\mu_r = 1$. The magnitude of the electric field computed by COMSOL at 1 MHz and 10 MHz is shown in Fig. 2(b) and 2(c), respectively. The figures show that the TEM fields decay significantly before reaching the end of the coaxial. This ensures that there is no reflected field that reaches back to the feed and therefore the measured impedance Z follows the one described by (5). By comparing Fig. 2(b) to Fig. 2(c) and comparing the value of γ at 1 MHz to the one at 10 MHz, one can see that higher frequency leads to a faster decay. This means that a shorter structure can be used at higher frequencies. Note that when the frequency is increased, a and b should be made smaller to avoid the generation of higher-order modes on the coaxial structure.

The phase angle of the simulated impedance is shown in Fig. 2(d). The CPZ is 220 kHz – 465 MHz with an average phase angle of 43.92° and PAD of ±3.22°. At lower frequencies, the TEM mode fields do not decay enough resulting in a strong reflection from the end of the structure and the wave impedance cannot be approximated as shown in (5). Consequently, half-integer inductive behavior is not observed anymore [37]. As the frequency increases, the stronger decay leads to a negligible reflection, and therefore the phase angle of the impedance approaches the predicted 45°. However, at the high end of the CPZ, MQS approximation ($\sigma \gg \omega\epsilon$) is no longer valid and the phase angle is no longer constant. Fig. 2(e) plots the amplitude of the impedance. As expected, within the CPZ, the slope of the line fitted to the amplitude-frequency data in the logarithmic scale has a slope of 0.49, which verifies the half-order fractional inductive behavior.

To form a complete assessment of the proposed design method, the effects of the device geometry and the electrical properties of the filling material on the device response are discussed next. Simulated amplitude and phase angle responses of the impedance with different conductivity and permeability values are shown in Fig. 3(a) – (b) and 3(c) – (d), respectively and the effect of different device lengths is demonstrated in Fig. 3(e) – (f).

First, the amplitude of the impedance is determined by the ratio of the shell radius to the core radius and the permeability and the conductivity of the filling medium, as shown in (4). As illustrated in Fig. 3(a), 3(c), and 3(e), a lower conductivity and a higher permeability lead to a higher impedance amplitude which is independent of the device length (as long as the frequency is high or the device length is long enough to ensure a small reflection from the end).

Second, the lower boundary of the working frequency range is controlled by the propagation constant γ and the length of the device as discussed previously using (6) in (2), one can show that the amplitude of the fields reaching the end

of the devices decays with:

$$e^{-Re\{\gamma\}l} \approx e^{-\sqrt{\pi f_{low}\mu\sigma}l} = A_{low}, \tag{7}$$

where f_{low} is the lower boundary of the frequency range. Here, A_{low} is a measure of the reflected fields' amplitude. As expressed (7), higher conductivity and permeability lead to a shorter device if A_{low} and f_{low} are kept the same. Indeed, Fig. 3(b) shows that doubling the length of the device while reducing the conductivity to its one-fourth yields the same low-frequency ($f \leq 10^5$) behavior. A similar effect with the permeability is observed in Fig. 3(d).

Third, the higher boundary of the working frequency range is limited by the MQS condition $\sigma \gg 2\pi f_{high}\epsilon$. Clearly, the higher boundary of the working frequency range as denoted by f_{high} is a function of the conductivity and permittivity. As it can be observed from Fig. 3(b), 3(d), and 3(f) that the higher boundary of the working frequency range only depends on the conductivity of the filling medium, and is independent of the length and permeability of the device.

Lastly, the effect of the deviation in the position of the core on the device response is demonstrated. This imperfection is the most obvious one during the device fabrication. As shown in Fig. 3(g) and 3(h), the impedance (both amplitude and phase angle) of the device is not sensitive to the deviation in the position of the core wire, showing the robustness of our proposed design technique.

III. EXPERIMENTAL VERIFICATION

To further verify our prediction, a prototype with the same geometry dimensions and material properties used in the simulations is fabricated. The inner wire and outer shell are made of copper. The filling material is sodium chloride (NaCl) water solution with a concentration of 0.2 g/mL corresponding to a conductivity of 20 S/m [47]. Deionized (DI) water is used to prepare the NaCl solution where the molar mass of NaCl is 58.44277 g/mol. The solution is kept in the laboratory conditions with the temperature of 22°C and relative humidity of 60%. The fabricated structure is fed through a 0.3 mm subminiature version A (SMA) connector and it is characterized using an Agilent E8363C Network Analyzer. Standard calibration tests (open, short, and load) of the Agilent 85052D 3.5 mm are performed to calibrate the instrument. The input power level of the Analyzer is set to –17 dBm. Considering the characteristic impedance 50 Ω of the whole measuring system, the frequency response is measured by defining the impedance Z = 50·[(1 + S11) / (1- S11)]. The measured phase angle and amplitude of the impedance are shown in Fig. 4(a) and 4(b), respectively. The impedance of the prototype has a phase angle averaged at 47.6° with a pseudo-inductance of 45.6 μH·s$^{-0.47}$ in the frequency range of 18 MHz – 1 GHz. The value of the pseudo-inductance value calculated via linear fitting is 67.2 μH·s$^{-0.5}$. As shown in reference [48], the strength of the electrolysis reaction decreases as the excitation frequency increases. Since at the lowest frequency, the measured phase of the impedance matches our prediction of (45°), the effect of the electrolysis

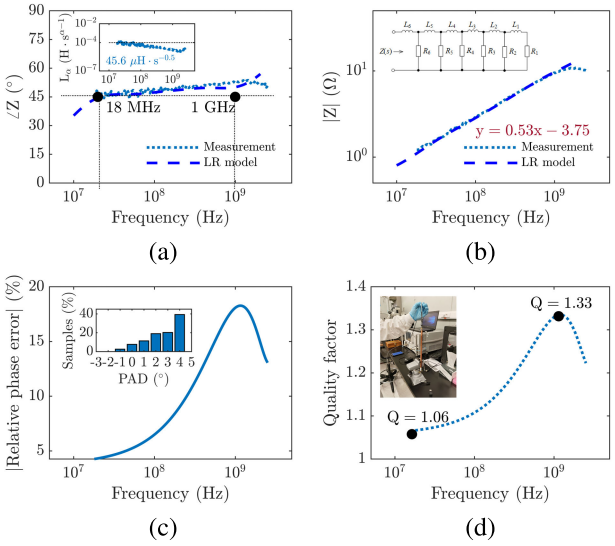

FIGURE 4. (a) Measured and equivalent RL model phase angle of the impedance with the pseudo-inductance shown in the inset, (b) measured and equivalent RL model amplitude of the impedance with a linear fitted equation inside the figure, (c) relative phase errors and corresponding normalized histograms (%) of phase angle deviation from CPA as inset, (d) quality factor with a measurement set-up shown in inset. Phase responses are optimized in the frequency range of 18 MHz – 1 GHz.

reaction can be neglected. Furthermore, the slope of the fitted impedance amplitude-frequency line is 0.53, demonstrating a half-order fractional inductive behavior. An FOI can be represented by series or parallel connected passive inductors and resistors [12]. The equivalent model of the proposed FOI is given as an inset of Fig. 4(b) and its frequency response in Fig. 4(a) and (b). The series inductance is L_n = {0.1 fH; 9.03 nH; 7.46 fH; 4.83 nH; 2.58 nH; 0.76 nH} while parallel resistance is R_n = {2.62; 2.30; 2.24; 23.65; 3.22; 8.06} Ω. The maximum PAD and relative phase errors in the half-order are 5° and 17%, respectively and shown in Fig. 4(c). The quality factor Q is calculated using $\frac{Im[Z]}{Re[Z]}$ and shown in Fig. 4(d). The maximum and minimum value of Q are found to be 1.3 and 1 which are close to the measurement results 1.33 and 1.06. The measurement set-up and the prototype are shown in the inset of Fig. 4(d).

IV. FRACTIONAL-ORDER PARALLEL $RL_\alpha C$ RESONATOR

In recent years, the increasing number of studies related to the application of fractional calculus is exceptional in many areas of science and engineering [25]–[29]. Thus, in this section, the performance of the realized FOI is verified through its application in the fractional-order parallel $RL_\alpha C$ resonance circuit. The impedance function of the circuit in Fig. 5 is given by:

$$Z(s) = \frac{s^\alpha \frac{1}{C}}{s^{1+\alpha} + s^\alpha \frac{1}{RC} + \frac{1}{CL_\alpha}}. \tag{8}$$

From (8) it can be seen that depending on the choice of the parameters L_α, C, and α, the equivalent impedance could

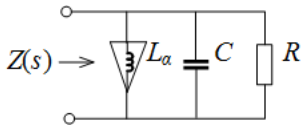

FIGURE 5. Parallel $RL_\alpha C$ resonance circuit.

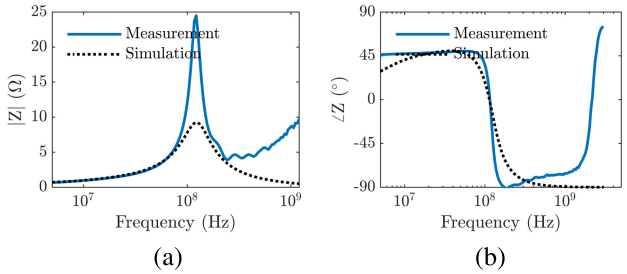

FIGURE 6. Impedance measurements of (a) magnitude and (b) phase response of parallel $L_\alpha C$ resonance.

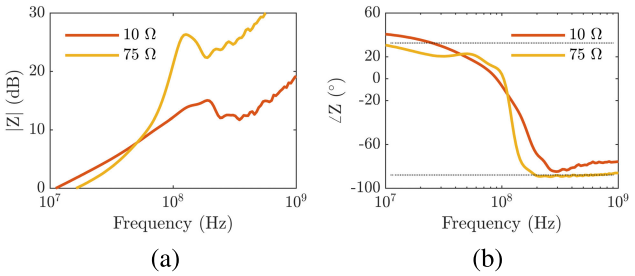

FIGURE 7. Fractional-order parallel $RL_\alpha C$ resonance response (a) gain and (b) phase for $R = \{10; 75\}$ Ω.

be pure imaginary or real at a certain frequency [21]. Thus, the circuit may act as the FOI or integer-order capacitor (L_α, C), and positive or negative resistor ($+R$, $-R$). If the sum of orders less than two ($1 + \alpha < 2$), then the phase response will be in the region of inductive and capacitive acute angle. The resonance angular frequency ω_{res} is obtained for $\mathrm{Im}\{(Z(j\omega)\} = 0$ which yields;

$$\omega_{res} = \left(\frac{sin(\frac{\alpha\pi}{2})}{CL_\alpha}\right)^{\frac{1}{1+\alpha}}, \tag{9}$$

where actually equal to pure real angular frequency (ω_{pr}). According to (9), the order α has high impact on ω_{res}. As α gets closer to zero, ω_{res} become very high and as α increases, ω_{res} decreases until the minimum value. The real impedance from (8) is obtained at ω_{res} and expressed as $Z_{real} = \frac{\omega^\alpha RL_\alpha}{\omega^\alpha L_\alpha + Rcos(\frac{\alpha\pi}{2})}$.

The performance of the fractional-order parallel $L_\alpha C$ resonance circuit has been verified experimentally using Agilent E4982A RF LCR meter (1 MHz – 3 GHz). The value of the realized FOI is $L_\alpha = 16.9\ \mu\mathrm{H} \cdot s^{-0.45}$ at 122 MHz. Considering the CPZ of our device and the effect of capacitance on the operation frequency range, the RF-type capacitor [49] with a value of $C = 100$ pF is selected. The magnitude and phase responses from the measurement and simulation are shown in Fig. 6. The measured resonance frequency is $f_{res} = 122$ MHz while $Z_{real} = 24.82\ \Omega$ while the simulated resonance frequency as same as measured one however the $Z_{real} = 9.51\ \Omega$. This is due to the higher parallel capacitance considering the T-shape SMA connector to measure the circuitry. The resonator circuit from Fig. 5 was tested using different values of the resistor $R = \{10; 75\}\ \Omega$ and the already tested $L_\alpha C$ setup. The obtained responses of the equivalent circuit are demonstrated in Fig. 7. The lower the parallel resistance, it will have more effect in damping the circuit and thus the lower the quality factor Q.

V. CONCLUSION

In conclusion, a straightforward and robust method to design FOIs is developed for the first time in the literature. The proposed generates the fractional inductance response via the TEM mode generated on a coaxial structure filled with a highly conductive material. The impedance of the TEM mode at the feeding position scales with $(j\omega)^{0.5}$ and is the underlying mechanism for the fractional inductance response. The design method is verified by simulations and experiments and the effects of all major design parameters on the device response are demonstrated. The performance of the proposed FOI is verified through its application in the fractional-order parallel $RL_\alpha C$ resonance circuit, to confirm the electronic tuning capability of the circuit at high frequencies.

REFERENCES

[1] W. Scheider, "Theory of the frequency dispersion of electrode polarization. Topology of networks with fractional power frequency dependence," *J. Phys. Chem.*, vol. 79, no. 2, pp. 127–136, Jan. 1975.
[2] J. E. Bauerle, "Study of solid electrolyte polarization by a complex admittance method," *J. Phys. Chem. Solids*, vol. 30, no. 12, pp. 2657–2670, Dec. 1969.
[3] A. K. Jonscher, "The universal dielectric response," *Nature*, vol. 267, no. 5613, pp. 673–679, Jun. 1977.
[4] C. Rong and B. Zhang, "Fractional electromagnetic waves in circular waveguides with fractional-order inductance characteristics," *J. Electromagn. Waves Appl.*, vol. 33, no. 16, pp. 2142–2154, Nov. 2019.
[5] R. Caponetto, S. Graziani, F. L. Pappalardo, and F. Sapuppo, "Experimental characterization of ionic polymer metal composite as a novel fractional order element," *Adv. Math. Phys.*, vol. 2013, pp. 1–10, Jun. 2013.
[6] I. S. Jesus and J. A. T. Machado, "Fractional control of heat diffusion systems," *Nonlinear Dyn.*, vol. 54, no. 3, pp. 263–282, Nov. 2008.
[7] A. Elwakil, "Fractional-order circuits and systems: An emerging interdisciplinary research area," *IEEE Circuits Syst. Mag.*, vol. 10, no. 4, pp. 40–50, Nov. 2010.
[8] A. Atangana and J. F. Gómez-Aguilar, "Decolonisation of fractional calculus rules: Breaking commutativity and associativity to capture more natural phenomena," *Eur. Phys. J. Plus*, vol. 133, no. 4, p. 166, Apr. 2018.
[9] D. Baleanu, A. K. Golmankhaneh, A. K. Golmankhaneh, and R. R. Nigmatullin, "Newtonian law with memory," *Nonlinear Dyn.*, vol. 60, nos. 1–2, pp. 81–86, Apr. 2010.
[10] M. C. Tripathy, D. Mondal, K. Biswas, and S. Sen, "Experimental studies on realization of fractional inductors and fractional-order bandpass filters," *Int. J. Circuit Theory Appl.*, vol. 43, no. 9, pp. 1183–1196, Sep. 2015.
[11] I. Petras, Y. Chen, and C. Coopmans, "Fractional-order memristive systems," in *Proc. IEEE Conf. Emerg. Technol. Factory Autom.*, Sep. 2009, pp. 1–8.
[12] A. Kartci, A. Agambayev, M. Farhat, N. Herencsar, L. Brancik, H. Bagci, and K. N. Salama, "Synthesis and optimization of fractional-order elements using a genetic algorithm," *IEEE Access*, vol. 7, pp. 80233–80246, 2019.
[13] I. Podlubny, "Fractional-order systems and $PI^\lambda D^\mu$ controllers," *IEEE Trans. Autom. Control*, vol. 44, no. 1, pp. 208–214, Jan. 1999.

[14] D. A. John, S. Banerjee, and K. Biswas, "Nanocomposite material characterization of a solid-state fractional capacitor," *IEEE Trans. Electron Devices*, vol. 67, no. 3, pp. 1136–1142, Mar. 2020.
[15] Z. M. Shah and F. A. Khanday, "Analysis of disordered dynamics in polymer nanocomposite dielectrics for the realization of fractional-order capacitor," *IEEE Trans. Dielectr. Electr. Insul.*, vol. 28, no. 1, pp. 266–273, Feb. 2021.
[16] T. C. Haba, G. Ablart, T. Camps, and F. Olivie, "Influence of the electrical parameters on the input impedance of a fractal structure realised on silicon," *Chaos, Solitons Fractals*, vol. 24, no. 2, pp. 479–490, Apr. 2005.
[17] A. S. Elwakil, A. Agambayev, A. Allagui, and K. N. Salama, "Experimental demonstration of fractional-order oscillators of orders 2.6 and 2.7," *Chaos, Solitons Fractals*, vol. 96, pp. 160–164, Mar. 2017.
[18] Y. Jiang and B. Zhang, "High-power fractional-order capacitor with $1 < \alpha < 2$ based on power converter," *IEEE Trans. Ind. Electron.*, vol. 65, no. 4, pp. 3157–3164, Sep. 2018.
[19] G. Tsirimokou, C. Psychalinos, A. S. Elwakil, and K. N. Salama, "Electronically tunable fully integrated fractional-order resonator," *IEEE Trans. Circuits Syst. II, Exp. Briefs*, vol. 65, no. 2, pp. 166–170, Feb. 2018.
[20] I. S. Jesus and J. A. T. Machado, "Development of fractional order capacitors based on electrolyte processes," *Nonlinear Dyn.*, vol. 56, nos. 1–2, pp. 45–55, Apr. 2009.
[21] A. G. Radwan and K. N. Salama, "Passive and active elements using fractional $L_\beta C_\alpha$ circuit," *IEEE Trans. Circuits Syst. I, Reg. Papers*, vol. 58, no. 10, pp. 2388–2397, May 2011.
[22] M. S. Sarafraz and M. S. Tavazoei, "Passive realization of fractional-order impedances by a fractional element and RLC components: Conditions and procedure," *IEEE Trans. Circuits Syst. I, Reg. Papers*, vol. 64, no. 3, pp. 585–595, Mar. 2017.
[23] D. A. John, M. Aware, A. Junghare, and K. Biswas, "Performance analysis of solid-state fractional capacitor-based analog $PI^{\lambda}D^{\mu}$ controller," *Circuits, Syst., Signal Process.*, vol. 39, no. 4, pp. 1815–1830, 2020.
[24] A. Agambayev, S. P. Patole, M. Farhat, A. Elwakil, H. Bagci, and K. N. Salama, "Ferroelectric fractional-order capacitors," *ChemElectroChem*, vol. 4, no. 11, pp. 2807–2813, Nov. 2017.
[25] L. Kadlčík and P. Horsky, "A CMOS follower-type voltage regulator with a distributed-element fractional-order control," *IEEE Trans. Circuits Syst. I, Reg. Papers*, vol. 65, no. 9, pp. 2753–2763, Sep. 2018.
[26] C. A. Monje, B. M. Vinagre, V. Feliu, and Y. Chen, "Tuning and auto-tuning of fractional order controllers for industry applications," *Control Eng. Pract.*, vol. 16, no. 7, pp. 798–812, Jul. 2008.
[27] H. Sun, Y. Zhang, D. Baleanu, W. Chen, and Y. Chen, "A new collection of real world applications of fractional calculus in science and engineering," *Commun. Nonlinear Sci. Numer. Simul.*, vol. 64, pp. 213–231, Nov. 2018.
[28] A. Morand, X. Moreau, P. Melchior, M. Moze, and F. Guillemard, "CRONE cruise control system," *IEEE Trans. Veh. Technol.*, vol. 65, no. 1, pp. 15–28, Jan. 2016.
[29] G. B. H. Frej, X. Moreau, E. Hamrouni, A. Benine-Neto, and V. Hernette, "A multi-modes semi-active suspension control strategy for peugeot 308 RCZ vehicle," in *Proc. 28th Medit. Conf. Control Autom. (MED)*, Sep. 2020, pp. 200–205.
[30] A. Lopes and J. Tenreiro-Machado, "Fractional-order model of a nonlinear inductor," *Bull. Polish Acad. Sci. Tech. Sci.*, vol. 67, no. 1, pp. 61–67, 2019.
[31] S. Westerlund and L. Ekstam, "Capacitor theory," *IEEE Trans. Dielectr. Electr. Insul.*, vol. 1, no. 5, pp. 826–839, Oct. 1994.
[32] F. E. Terman, *Radio Engineer's Handbook*, 1st ed. New York, NY, USA: McGraw-Hill, Jan. 1943.
[33] J. F. Gómez-Aguilar, H. Yépez-Martínez, C. Calderón-Ramón, M. Benavidez-Cruz, and L. J. Morales-Mendoza, "Fractional electromagnetic waves in conducting media," *J. Electromagn. Waves Appl.*, vol. 30, no. 2, pp. 259–271, Jan. 2016.
[34] J. F. Gómez-Aguilar, H. Yépez-Martínez, R. F. Escobar-Jiménez, C. M. Astorga-Zaragoza, L. J. Morales-Mendoza, and M. González-Lee, "Universal character of the fractional space-time electromagnetic waves in dielectric media," *J. Electromagn. Waves Appl.*, vol. 29, no. 6, pp. 727–740, Apr. 2015.
[35] B. Zhang, R. Huang, and D. Qiu, "Fractional order series resonance system for wireless electric energy transmission," U.S. Patent 9 620 965, Apr. 11, 2017.
[36] J. A. T. Machado and A. M. S. F. Galhano, "Fractional order inductive phenomena based on the skin effect," *Nonlinear Dyn.*, vol. 68, nos. 1–2, pp. 107–115, Apr. 2012.
[37] N. A.-Z. R-Smith, A. Kartci, and L. Brančík, "Application of numerical inverse laplace transform methods for simulation of distributed systems with fractional-order elements," *J. Circuits, Syst. Comput.*, vol. 27, no. 11, Oct. 2018, Art. no. 1850172.
[38] I. Schäfer and K. Krüger, "Modelling of lossy coils using fractional derivatives," *J. Phys. D, Appl. Phys.*, vol. 41, no. 4, Feb. 2008, Art. no. 045001.
[39] R. Lerner, "The design of a constant-angle or power-law magnitude impedance," *IEEE Trans. Circuit Theory*, vol. CT-10, no. 1, pp. 98–107, Mar. 1963.
[40] G. Tsirimokou, A. Kartci, J. Koton, N. Herencsar, and C. Psychalinos, "Comparative study of discrete component realizations of fractional-order capacitor and inductor active emulators," *J. Circuits, Syst. Comput.*, vol. 27, no. 11, Oct. 2018, Art. no. 1850170.
[41] R. Sotner, J. Jerabek, A. Kartci, O. Domansky, N. Herencsar, V. Kledrowetz, B. B. Alagoz, and C. Yeroglu, "Electronically reconfigurable two-path fractional-order PI/D controller employing constant phase blocks based on bilinear segments using CMOS modified current differencing unit," *Microelectron. J.*, vol. 86, pp. 114–129, Apr. 2019.
[42] M. F. Tolba, L. A. Said, A. H. Madian, and A. G. Radwan, "FPGA implementation of the fractional order integrator/differentiator: Two approaches and applications," *IEEE Trans. Circuits Syst. I, Reg. Papers*, vol. 66, no. 4, pp. 1484–1495, Apr. 2019.
[43] C. Muñiz-Montero, L. V. García-Jiménez, L. A. Sánchez-Gaspariano, C. Sánchez-López, V. R. González-Díaz, and E. Tlelo-Cuautle, "New alternatives for analog implementation of fractional-order integrators, differentiators and PID controllers based on integer-order integrators," *Nonlinear Dyn.*, vol. 90, no. 1, pp. 241–256, Oct. 2017.
[44] A. Adhikary, S. Choudhary, and S. Sen, "Optimal design for realizing a grounded fractional order inductor using GIC," *IEEE Trans. Circuits Syst. I, Reg. Papers*, vol. 65, no. 8, pp. 2411–2421, Aug. 2018.
[45] A. Soltan, A. G. Radwan, and A. M. Soliman, "Fractional-order mutual inductance: Analysis and design," *Int. J. Circuit Theory Appl.*, vol. 44, no. 1, pp. 85–97, Jan. 2016.
[46] J.-M. Jin, *Theory and Computation of Electromagnetic Fields*. Hoboken, NJ, USA: Wiley, 2011.
[47] F. Rajabipour, J. Weiss, and D. M. Abraham, "Insitu electrical conductivity measurements to assess moisture and ionic transport in concrete (a discussion of critical features that influence the measurements)," in *Proc. Int. RILEM Symp. Concrete Sci. Eng., Tribute Arnon Bentur*, Paris, France, 2004, pp. 1–18.
[48] S. Marsh, "On alternating current electrolysis," *Proc. Roy. Soc. A*, vol. A97, no. 687, pp. 124–144, 1920.
[49] *Datasheet: Kemet Electronics Corporation 'HiQ-CBR Series, 0402 C0G Dielectric, Low ESR 6.3–500 VDC, 1 MHz – 50 GHz (RF & Microwave)*, document C1030_C0G_CBR, Rev. 6/8/2018. [Online]. Available: https://goo.gl/fdpbQ8

LI ZHANG (Student Member, IEEE) received the B.S. degree in microelectronic science and engineering from the University of Electronic Science and Technology of China, China, in 2018, and the M.S. degree in electrical engineering from the King Abdullah University of Science and Technology, Thuwal, Saudi Arabia, in 2019, where he is currently pursuing the Ph.D. degree in electrical engineering. His research interests include modeling, designing, and the application of fractional-order circuit elements.

ASLIHAN KARTCI (Member, IEEE) received the M.S. degree in electronics from Yildiz Technical University, Turkey, in 2015, and the Ph.D. degree from the Department of Radio Electronics, Brno University of Technology, Czech Republic, in 2019. Since January 2020, she has been with the King Abdullah University of Science and Technology (KAUST), Thuwal, Saudi Arabia, where she is currently a Postdoctoral Fellow. Her research interests include fractional-order analog integrated circuits with modern active elements, and their application as oscillators and filters, general element simulator, numerical methods for analysis of electronic networks, and computer-aided methods for the simulation of electronic circuits for high-frequency applications.

AHMED ELWAKIL (Senior Member, IEEE) was born in Cairo, Egypt. He received the B.Sc. and M.Sc. degrees in electronics and communications from Cairo University, Egypt, and the Ph.D. degree in electrical and electronic engineering from the National University of Ireland, University College Dublin. He also held visiting positions at Istanbul Technical University, Turkey, Queens University, Belfast, U.K., the Technical University of Denmark, Lyngby, Denmark, and the King Abdullah University of Science and Technology, Saudi Arabia. He is currently a Full Professor with the University of Sharjah, United Arab Emirates. He is also with the University of Calgary, Calgary, AB, Canada. He is also with the Nanoelectronics Integrated Systems Center (NISC) Research Center, Nile University, Cairo. He has authored or coauthored more than 350 publications in these areas (current H-index 45). His research interests include circuit theory, nonlinear dynamics, chaos theory, and fractional-order circuits and systems with diverse applications ranging from the modeling of oscillatory networks and nonlinear behavior in electronic circuits and plasma physics to modeling of energy storage devices, bio-materials, and biological tissues. Since 2000, he has been a member of the IEEE Technical Committee on Nonlinear Circuits and Systems. He was a recipient of the Egyptian Government First Class Medal for achievements in engineering sciences, in 2015, and the UAE President Award (Khalifa Award), in 2020. He is an International Observer in the European Cooperation in Science and Technology (COST) action on fractional-order system-analysis synthesis and their importance for future design (CA15225) and an Expert with the United Nations Development Program (UNDP). He was on the Editorial Board of the IEEE JOURNAL ON EMERGING AND SELECTED TOPICS IN CIRCUITS AND SYSTEMS. He was an Associate Editor of the IEEE TRANSACTION ON CIRCUITS AND SYSTEMS—I: REGULAR PAPERS. He also serves as an Editor-in-Chief for the *International Journal of Circuit Theory and Applications* (Wiley) and an Associate Editor for the *International Journal of Electronics and Telecommunications* (AEUE) (Elsevier).

HAKAN BAGCI (Senior Member, IEEE) received the B.S. degree in electrical and electronics engineering from Bilkent University, Ankara, Turkey, in 2001, and the M.S. and Ph.D. degrees in electrical and computer engineering from the University of Illinois at Urbana- Champaign (UIUC), Urbana, IL, USA, in 2003 and 2007, respectively.

From June 1999 to July 2001, he worked as an Undergraduate Researcher with the Computational Electromagnetics Group, Bilkent University. From August 2001 to December 2006, he was a Research Assistant with the Center for Computational Electromagnetics and Electromagnetics Laboratory, UIUC. From January 2007 to August 2009, he was a Research Fellow with the Radiation Laboratory, University of Michigan, Ann Arbor, MI, USA. Since August 2009, he has been with the King Abdullah University of Science and Technology (KAUST), Thuwal, Saudi Arabia, where he is currently an Associate Professor of electrical engineering. He authored or coauthored 90 journal articles and 200 papers in conference proceedings. His research interests include various aspects of theoretical and applied computational electromagnetics with emphasis on well-conditioned frequency and time domain integral equation formulations and their discretization, hybrid time domain integral and differential equation solvers, accurate, stable, and efficient marching schemes for time domain solvers, stochastic characterization of electromagnetic field and wave interactions on complex geometries, and solution of two and three dimensional electromagnetic inverse scattering problem using signal processing techniques.

Dr. Bagci was a recipient of the 2008 International Union of Radio Scientists (URSI) Young Scientist Award and the 2004–2005 Interdisciplinary Graduate Fellowship from the Computational Science and Engineering Department, UIUC. His paper titled Fast and Rigorous Analysis of EMC/EMI Phenomena on Electrically Large and Complex Structures Loaded With Coaxial Cables was one of the three finalists (with honorable mention) for the 2008 Richard B. Schulz Best Transactions Paper Award given by the IEEE Electromagnetic Compatibility Society. He authored (as a student) or coauthored (as a student and an advisor) 17 finalist/honorable mention papers in the student paper competitions at the 2005, 2008, 2010, 2014, 2015, 2016, 2017, 2018 IEEE Antennas and Propagation Society International Symposiums, and 2013, 2014, 2016, 2017, and 2018 Applied Computational Electromagnetics Society Conferences.

KHALED N. SALAMA (Senior Member, IEEE) received the B.S. degree from the Department Electronics and Communications, Cairo University, Cairo, Egypt, in 1997, and the M.S. and Ph.D. degrees from the Department of Electrical Engineering, Stanford University, Stanford, CA, USA, in 2000 and 2005, respectively.

From 2005 to 2009, he was an Assistant Professor with the Rensselaer Polytechnic Institute, Troy, NY, USA. He joined the King Abdullah University of Science and Technology (KAUST), in January 2009, where he is currently a Professor. He was the Founding Program Chair, in August 2011. He is the Director of the sensors initiative a consortium of nine universities, such as KAUST, MIT, UCLA, GATECH, MIT, UCLA, Brown University, Georgia Tech, TU Delft, Swansea University, the University of Regensburg, and the Australian Institute of Marine Science (AIMS). His work on CMOS sensors for molecular detection has been funded by the National Institutes of Health (NIH) and the Defense Advanced Research Projects Agency (DARPA), awarded the Stanford-Berkeley Innovators Challenge Award in biological sciences and was acquired by Lumina Inc. He is the author of 250 articles and 20 U.S. patents on low-power mixed-signal circuits for intelligent fully integrated sensors and neuromorphic circuits using memristor devices.